PAPER SUBMITTED FOR POSSIBLE PUBLICATION

IN EARTHQUAKE ENGINEERING AND STRUCTURAL DYNAMICS

A cantilever beam analogy for quantifying higher mode effects in multistorey buildings

by

Lydell Wiebe and Constantin Christopoulos

Contact Author:

Lydell Wiebe
Department of Civil Engineering, McMaster University, Canada
1280 Main Street W, Hamilton ON, L8S 4L7
E-mail: wiebel@mcmaster.ca

Submitted October 2013

Revised July 2014

A cantilever beam analogy for quantifying higher mode effects in multistorey buildings

by

Lydell Wiebe[1] and Constantin Christopoulos[2]

Summary

This paper examines higher mode effects in systems where the ductile mechanism for seismic design is the base moment-rotation response. The modal properties of flexural and shear beams with uniform mass and elasticity and with a variable amount of base rotational restraint are derived. As the base fixity is released, the first mode becomes the rigid body rotation of the beam about the base, but the higher modes change much less, particularly for the shear beam model. Most response quantities that are of interest in the seismic design of typical mid-rise buildings are controlled by the first two lateral modes, except at locations along the height where the second mode contributes little. However, the third and higher lateral modes are more significant for high-rise buildings.

Based on the theory of uniform cantilever shear beams, expressions are developed that avoid the need for a modal analysis to estimate the overturning moment, storey shear, and floor acceleration envelopes. Considering the measured response from shake table testing of a large-scale eight-storey controlled rocking steel braced frame, the proposed expressions are shown to be of similar or better accuracy to a modified modal superposition technique, which combines the higher-mode response from an elastic modal analysis with the response associated with achieving the maximum base overturning moment according to an inverted triangular load distribution. Since the proposed method uses only parameters that are available at the initial design stage, avoiding analysis of a structural model, it is likely to be especially useful for preliminary design.

Keywords: higher mode effects, dynamic amplification, capacity design, self-centering systems, controlled rocking steel braced frames, reinforced concrete shear walls

INTRODUCTION

Capacity design, first proposed by Park and Paulay [1], attempts to make the seismic force demands on a structural system independent of the ground motion intensity. A nonlinear mechanism is specified by the designer and is proportioned to have a certain strength, which may be determined using various force-based [e.g. 2] or displacement-based [e.g. 3] approaches. Once the mechanism has been designed, all other elements of the structural system are designed to elastically resist the maximum forces that are consistent with the nonlinear mechanism at its maximum deformed state, with due consideration of strain hardening of steel, material overstrength, system overstrength, and appropriate factors of safety. By doing this, the intent is that an increase in the ground motion intensity will increase the deformation demand on the nonlinear mechanism, but will not significantly increase the force demand on the other elements of the structural system, especially those that ensure the integrity of the vertical load carrying system.

[1] Assistant Professor, Dept. of Civil Engineering, McMaster University, Hamilton, ON, Canada. Email: wiebel@mcmaster.ca
[2] Professor, Dept. of Civil Engineering, University of Toronto, Toronto, ON, Canada.

Whereas the intent of capacity design is to limit the structural forces by forming a nonlinear mechanism, higher mode effects work against this by increasing the structural forces even after that mechanism has formed. Higher mode effects are known to be particularly significant for reinforced concrete (RC) walls, where the nonlinear mechanism is intended to be the formation of a plastic hinge at the wall base, because a wall with a base rotational joint has multiple lateral force distributions that satisfy its boundary conditions but that produce larger forces along the height than a first-mode distribution. These higher mode effects were first identified by Blakeley et al. [4], and studies since then have demonstrated this behaviour through more refined numerical modelling [5-11]. Higher mode effects have also been observed in shake table tests of reinforced concrete walls [12-14]. An extensive bibliography on research regarding higher mode effects on shear forces in reinforced concrete walls has been provided by Rutenberg [15].

Many recommendations have been made for adapting modal analysis tools to quantify higher mode effects in RC walls. Eibl and Keintzel [16] introduced the concept of modal limit forces, which are the maximum forces that could be developed in each mode with elastic-perfectly-plastic yielding, and proposed designing for the square-root-of-the-sum-of-squares (SRSS) combination of the lesser of the modal limit force and the elastic demand for each mode. For simplified dynamic analysis, they developed an approximate expression to calculate the base shear by combining the modal limit force in the first mode with the elastic force in the second mode. Keintzel [17] later compared the modal periods and displaced shapes for flexural cantilevers with varying base rotational stiffness, concluding that the properties of the higher modes are not sensitive to the base rotational restraint and thus the elastic modal properties can be used to estimate the influence of higher modes in the nonlinear range. Priestley and Amaris [8] adapted this procedure by calculating the first-mode properties using the direct displacement-based design lateral force distribution while using the elastic properties of the higher modes, and Priestley et al. [3] developed an approximation to these envelopes that does not require modal analysis. Panagiotou and Restrepo [13] suggested that the higher mode effects are mostly due to the second lateral mode. Accordingly, they proposed a modal combination of the reduced first-mode envelopes of shear and moment with envelopes that are based on a polynomial approximation to the elastic second-mode shape.

Other researchers have considered the influence of stiffness reductions in the structure. Kowalsky [18] proposed Effective Modal Superposition for bridge design, where the properties of the higher modes are calculated using the secant stiffness of elements at the maximum expected displacement and combined using an SRSS approach. Sullivan et al. [19] proposed combining the first-mode forces that reach the base overstrength moment with higher-mode forces based on Transitory Inelastic Modes (TIMs), which are found by modelling all plastic hinges as pins. Pennucci et al. [20] found that a similar approach worked well for tall RC walls with varying degrees of coupling. That study also presented a simplified Weighted Capacity Design approach that did not require modal analysis, but instead calculated design envelopes at key points along the structural height based on a combination of closed-form solutions for flexural beams with fixed and pinned bases.

Recently, other systems have been proposed that also rely on a nonlinear base moment-rotation response to limit the seismic forces. Controlled rocking systems allow part of the structure to lift off the foundation in response to lateral loads, resulting in a nonlinear response that is controlled using post-tensioning or supplemental energy dissipation. Recent studies of controlled rocking steel braced frames have demonstrated that the peak seismic forces for frame members are

strongly influenced by higher mode effects [21-25]. These effects must be considered, either by designing to resist them elastically [21-23], or by mitigating them using multiple mechanisms [24-25].

The purpose of this paper is to investigate the influence of base fixity on the modal properties of cantilever-type structures, to examine the relative influence of the higher modes on key response parameters, and to derive a simple way to estimate seismic design forces in systems with a non-linear base moment-rotation response. Unlike previous studies, the modal properties of cantilevered beams with uniform mass and elasticity are derived for both flexural and shear beams, and the base rotational restraint is taken as variable, allowing the influence of this parameter on key performance indices to be studied using a response spectrum analysis approach. The modal equations for a shear beam are used to develop design equations for controlled rocking steel braced frames. By using the nondimensional modal properties of a cantilever shear beam, the proposed equations remove the need for the designer to conduct a modal analysis, and thus these equations are intended to be usable for preliminary design before a structural model can be developed. The proposed equations are compared to results from shake table testing. Although this part of the paper focuses on controlled rocking steel braced frames, it is also expected to apply to other systems with primarily shear-type deformations and a nonlinear base moment-rotation response.

ANALOGY TO CANTILEVER BEAMS WITH DISTRIBUTED MASS AND ELASTICITY

As shown in Figure 1, the response of a lateral load resisting system may be dominated by flexural-type deformations (e.g. slender reinforced concrete shear wall) or by shear-type deformations (e.g. mid-rise steel concentrically braced frame). A seismic force resisting system that is fixed at the base may lose rotational stiffness at times during seismic loading, whether by rocking at the base of a controlled rocking system, or by forming a plastic hinge at the base of a reinforced concrete shear wall. As the system vibrates, the base rotational restraint fluctuates in a range between a fixed condition and a pinned condition. The incremental response at each time instant is subject to the structural properties and boundary conditions at that instant.

A medium- to high-rise structure with this kind of behaviour can be generalised by considering the cantilever beam with uniform mass and elasticity that is shown in Figure 2a. According to Timoshenko beam theory [26], each section of the beam (Figure 2b) develops flexural curvatures (ϕ in Figure 2c) and shear strains (γ in Figure 2d), and the flexural curvatures accumulate to produce a rigid-body flexural rotation (θ in Figure 2e). Timoshenko assumed that the rate of change of deformation over the height, $\partial x/\partial z$, is given by:

$$\partial x/\partial z = \theta + \gamma \tag{1}$$

The mass of a building is typically distributed nearly uniformly over the height and does not rotate

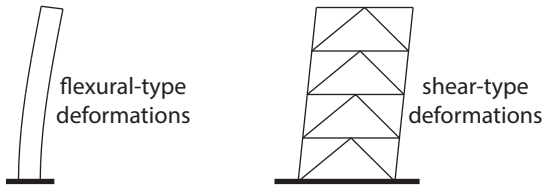

Figure 1 Systems with flexural-type and shear-type deformations

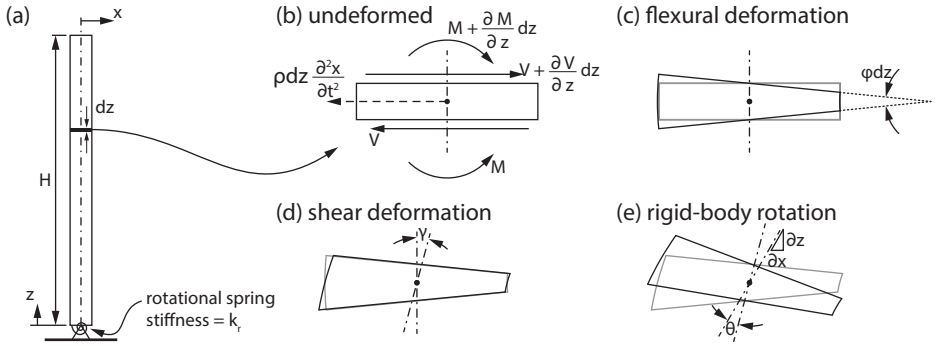

Figure 2 Beam with uniform mass and elasticity: (a) overall view; (b) undeformed section; (c) flexural deformation; (d) additional shear deformation; (e) additional rigid body rotation

about an axis in the horizontal plane. Although the stiffness of most real buildings varies over the height, uniform stiffness is assumed in order to focus on the effects of the base rotational stiffness. With these assumptions, Timoshenko beam theory [26] can be simplified to two equations for two bounds of behaviour. First, if shear deformations are small relative to flexural deformations, $\gamma = 0$ and Eq. (1) can be written as Eq. (2), which is the equation of motion for a flexural beam [27]. Second, if flexural deformations are relatively small, Eq. (3) can be developed as the equation of motion for a shear beam. Although the following discussion considers only these extremes, it could be extended by considering combinations of flexural and shear beams [e.g. 28].

$$EI\left(\partial^4 x/\partial z^4\right)+\rho A\left(\partial^2 x/\partial t^2\right)=0 \tag{2}$$

$$\left(\partial^2 x/\partial z^2\right)-\left(\rho/\kappa G\right)\left(\partial^2 x/\partial t^2\right)=0 \tag{3}$$

In Eqs. (2)-(3), t is time, E is the modulus of elasticity of the beam, I is its second moment of area about the axis of bending, ρ is its mass density (kg/m^3 in SI units), A is its cross-sectional area, G is its shear modulus, and κ is a sectional constant that accounts for the non-uniform distribution of shear stresses on the section.

Solution to modal equations for flexural beam

Following classical techniques [27], the solution to the equation of motion for both the flexural beam and the shear beam is assumed to be of the form:

$$x_n\left(z,t\right)=\phi_n\left(z\right)q_n\left(t\right) \tag{4}$$

where $x_n\left(z,t\right)$ is the displacement in mode n, $\phi_n\left(z\right)$ is the n^{th} mode shape and $q_n\left(t\right)$ describes the response of mode n over time in displacement units. Figure 2 shows the boundary conditions and their sign conventions: the top is free and the base has a linear rotational spring with stiffness k_r. For a flexural beam, the base rotational restraint results in the following boundary condition:

$$k_r\phi_n'\left(0\right)=EI\phi_n''\left(0\right) \tag{5}$$

where the prime symbol denotes a derivative with respect to z. The modal constant, β_n, is defined for mode n of a flexural beam as:

$$\beta_n{}^4 = \omega_n{}^2 \rho A / EI \tag{6}$$

A non-dimensional rotational restraint parameter is defined for the flexural beam as:

$$R_f = k_r H / EI \tag{7}$$

The mode shape can then be solved from Eq. (2) with an arbitrary constant C_n as:

$$\phi_n(z) = C_n \left(\cosh \beta_n z - \cos \beta_n z + A_{n,\sin} \sin \beta_n z - A_{n,\sinh} \sinh \beta_n z \right) \tag{8}$$

where $A_{n,\sin}$ and $A_{n,\sinh}$ are:

$$A_{n,\sin} = \left[\cos \beta_n H + \cosh \beta_n H + 2 \left(\beta_n H / R_f \right) \sinh \beta_n H \right] / \left(\sin \beta_n H + \sinh \beta_n H \right) \tag{9}$$

$$A_{n,\sinh} = \left[\cos \beta_n H + \cosh \beta_n H - 2 \left(\beta_n H / R_f \right) \sinh \beta_n H \right] / \left(\sin \beta_n H + \sinh \beta_n H \right) \tag{10}$$

and where the frequency equation is given by:

$$1 + \left(\cos \beta_n H \right) \left(\cosh \beta_n H \right) - \left(\beta_n H / R_f \right) \left[\left(\sin \beta_n H \right) \left(\cosh \beta_n H \right) - \left(\cos \beta_n H \right) \left(\sinh \beta_n H \right) \right] = 0 \tag{11}$$

Table 1 gives the values of $\beta_n H$ that satisfy Eq. (11) with a fixed base ($R_f \to \infty$) and a pinned base ($R_f = 0$). These values and the mode shapes given by Eq. (8) are equivalent to the expressions developed by Young and Felgar [29] for these limiting cases of base rotational restraint, but these expressions also encompass the full range of intermediate restraint conditions. The modes associated with $R_f = 0$ are the TIMs [19] for a flexural beam with uniform mass and stiffness.

Solution to modal equations for shear beam

The shear force in the shear beam, V_n, is found by taking θ in Eq. (1) as constant over the height and equal to $\phi_n'(H) q_n(t)$ because the shear at the tip is zero:

$$V_n(z,t) = \kappa G A \gamma_n(z,t) = \kappa G A \left[\partial x_n / \partial z - \phi_n'(H) q_n(t) \right] \tag{12}$$

The base rotational restraint boundary condition can be written by using Eqs. (4) and (12) to integrate the shear force diagram over the height and equating this to the moment in the spring:

$$\kappa G A \int_0^H \left(\phi_n'(z) - \phi_n'(H) \right) dz = k_r \phi_n'(H) \tag{13}$$

The modal constant, β_n, is defined for mode n of a shear beam as:

Table 1 Frequency parameters $\beta_n H$ for cantilever beams with fixed and pinned base conditions

	flexural beam		shear beam	
mode	$R_f \to \infty$	$R_f = 0$	$R_v \to \infty$	$R_v = 0$
1	1.8751	0.0000	1.5708	0.0000
2	4.6941	3.9266	4.7124	4.4934
3	7.8548	7.0686	7.8540	7.7253
$n \to \infty$	$(2n-1)\pi/2$	$(n-1)\pi$	$(2n-1)\pi/2$	$(2n-1)\pi/2$

$$\beta_n{}^2 = \omega_n{}^2 \rho / \kappa G \tag{14}$$

The non-dimensional rotational restraint parameter is defined for the shear beam as:

$$R_v = k_r / \kappa GAH \tag{15}$$

The mode shape can then be solved from Eq. (3) as:

$$\phi_n(z) = C_n \sin \beta_n z \tag{16}$$

where C_n is an arbitrary constant and where the frequency equation is given by:

$$\beta_n H \cos \beta_n H - (\sin \beta_n H)/(1 + R_v) = 0 \tag{17}$$

Table 1 lists the values of $\beta_n H$ that satisfy Eq. (17) for the fixed base ($R_v \to \infty$) and pinned base ($R_v = 0$). The modes associated with $R_v = 0$ are the TIMs [19] for a shear beam with uniform mass and stiffness.

Modal displacements, shears, and moments

Figure 3 plots the properties of the first three modes of a cantilevered flexural beam for a range of nondimensional rotational restraint coefficients. The first column of plots shows the displaced shape $\Gamma_n \phi_n$ for the flexural beam, which does not depend on how the mode shape is normalized because the modal participation factor is defined as:

$$\Gamma_n = \frac{\int_0^H \phi_n(z) dz}{\int_0^H \phi_n^2(z) dz} \tag{18}$$

This assumes a uniform mass distribution. The normalised modal shear force is defined as:

$$\overline{V}_n(z) = H^3 \phi_n'''(z) = \frac{V_n(z,t) H^3}{EIq_n(t)} \tag{19}$$

The second column of Figure 3 shows $\Gamma_n \overline{V}_n(z)$ for the flexural beam, which is related to shear forces and is independent of both the normalization of the mode shape and the numerical values of the mass and stiffness of the beam. Similarly, the normalised modal moment $\overline{M}_n(z)$ is defined as:

$$\overline{M}_n(z) = H^2 \phi_n''(z) = \frac{M_n(z,t) H^2}{EIq_n(t)} \tag{20}$$

The third column of plots in Figure 3 shows $\Gamma_n \overline{M}_n(z)$ for the flexural beam.

Similarly, Figure 4 shows the modal properties of a shear beam. Eq. (12) is used to define $\overline{V}_n(z)$ for a shear beam as:

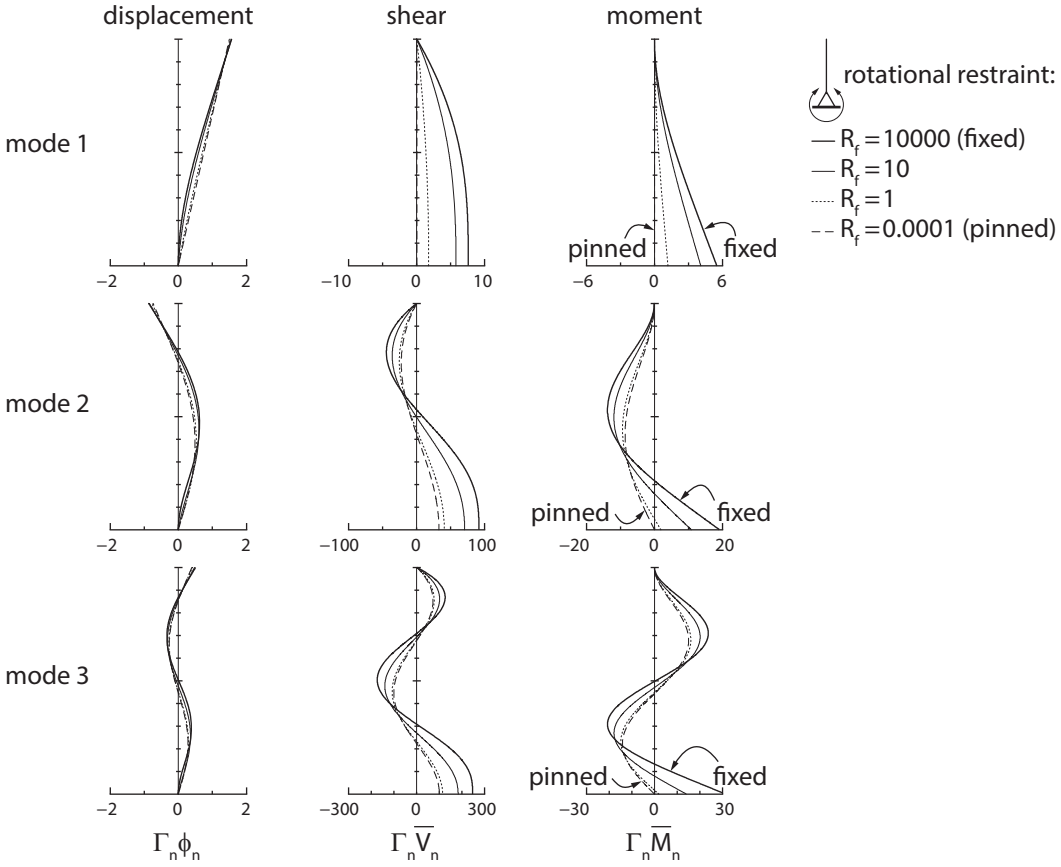

Figure 3 Properties of the first three modes of flexural beams with varying base fixity

$$\overline{V}_n(z) = H(\phi_n'(z) - \phi_n'(H)) = \frac{V_n(z,t)H}{\kappa G A q_n(t)} \tag{21}$$

The normalised modal moment $\overline{M}_n(z)$ is found by integrating the shear force diagram:

$$\overline{M}_n(z) = \phi_n(H) - \phi_n(z) - (H - z)\phi_n'(H) = \frac{M_n(z,t)}{\kappa G A q_n(t)} \tag{22}$$

Figure 3 and Figure 4 show that the displaced shape in each mode is not greatly affected by the amount of moment restraint at the base for either type of beam. As the base moment restraint is released, the first mode becomes the rigid body rotation of the beam about its base, and the shear and bending moment diagrams approach zero. However, the sectional forces for the higher modes do not approach zero as the restraint is released. For the flexural beam in the second mode, the shear forces reduce and the point of zero shear shifts downward, increasing the shear at some locations. Similarly, the bending moment diagram of the flexural beam in the second mode is generally reduced by releasing the base fixity, but the moments increase at some locations because of the changing location of contraflexure. Similar changes occur in the third and higher modes. For the shear beam, the sectional forces are less affected by the degree of base fixity than for the flexural beam. The shears near the base increase slightly as the restraint is released, while the bending moments reduce appreciably only in the lower half of the beam.

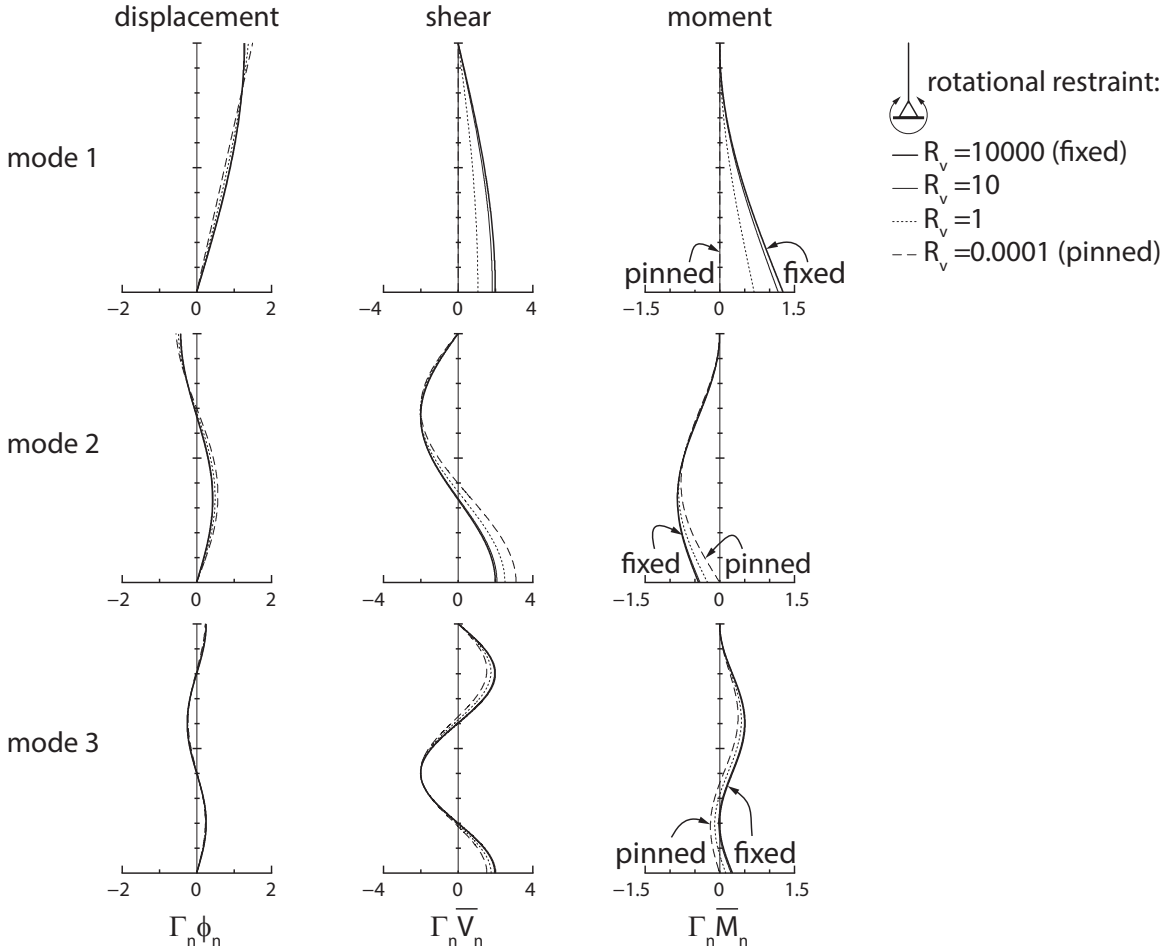

Figure 4 Properties of the first three modes of shear bams with varying base fixity

Modal periods

A nondimensional period is defined for the flexural beam as:

$$\overline{T}_{nf} = \frac{2\pi}{(\beta_n H)^2} = \frac{T_n}{H^2}\sqrt{\frac{EI}{\rho A}} \tag{23}$$

and for the shear beam as:

$$\overline{T}_{nv} = \frac{2\pi}{\beta_n H} = \frac{T_n}{H}\sqrt{\frac{\kappa G}{\rho}} \tag{24}$$

where T_n is the period of mode n, which is calculated using Eqs. (6) and (11) for the flexural beam, and Eqs. (14) and (17) for the shear beam. Table 2 gives $\overline{T}_{nf}$ and $\overline{T}_{nv}$ for the first three fixed-base modes, together with formulae that are accurate to three significant figures for the higher modes with $n > 3$; Young and Felgar [29] developed equivalent expressions for flexural beams, but not for shear beams. The ratios of the higher-mode periods to the first-mode period are also given. Figure 5 shows how the periods are affected by the base rotational restraint. For both

Table 2 Nondimensional periods of fixed-base cantilever beams

	flexural beam		shear beam	
mode	$\overline{T}_{nf}$	$\overline{T}_{1f}/\overline{T}_{nf}$	$\overline{T}_{nv}$	$\overline{T}_{1v}/\overline{T}_{nv}$
1	1.7870	1.0000	4.0000	1.0000
2	0.2852	6.2669	1.3333	3.0000
3	0.1018	17.5475	0.8000	5.0000
$n \to \infty$	$\dfrac{8}{\pi(2n-1)^2}$	$\dfrac{(2n-1)^2}{1.4250}$	$\dfrac{4}{2n-1}$	$2n-1$

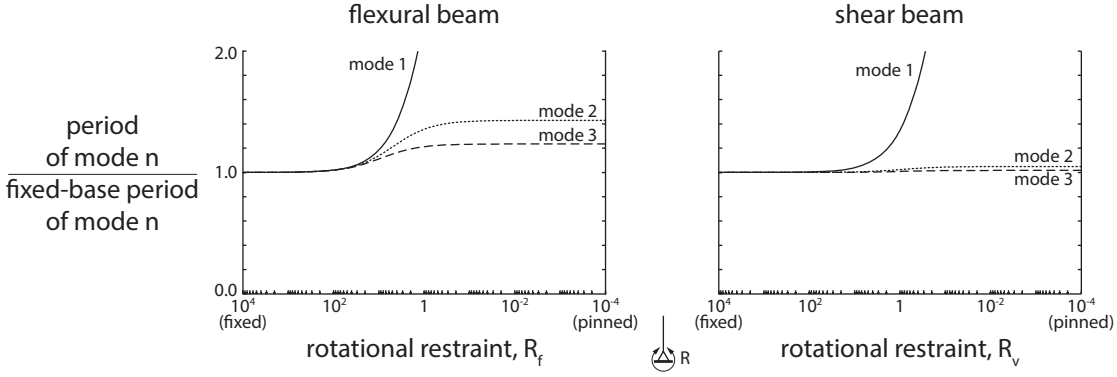

Figure 5 Effect of base fixity on modal periods of flexural and shear beams

system types, the first-mode period becomes unbounded as the base fixity is released. The higher-mode periods elongate but are bounded. For the flexural beam as the base becomes pinned, the second-mode period increases by 43% relative to the fixed-base period, while the third-mode period increases by only 23% and the higher modes have successively less change in period as the base fixity reduces. The periods of the higher modes of the shear beam are less affected by the base rotational restraint than they are for the flexural beam: none of the higher-mode periods of the shear beam increases by more than 5% as the base rotational restraint is released.

RELATIVE MODAL INFLUENCES ON NONLINEAR SEISMIC RESPONSE

Modal contributions to seismic response

The incremental nonlinear dynamic response of a structure at each instant is governed by the boundary conditions that apply at that time. As a structure with a nonlinear base moment-rotation response is driven further into its nonlinear range, less of the total response will occur in the fixed-base condition. Pennucci et al. [20] have proposed a capacity design procedure that is based on a weighted combination of modal responses assuming a fixed base and a pinned base. To further investigate the expected nonlinear dynamic response of multistorey buildings, the following section uses the modal properties that were developed above to show how the relative contribution of each mode to various response quantities is affected by the base rotational restraint.

The effective modal mass in each mode is defined as:

$$M_n^* = \Gamma_n \int_0^H \rho A \phi_n(z) dz \tag{25}$$

Given that the sum of effective modal masses is equal to the total mass [27], the contribution from each mode to the effective modal mass is calculated as $(\Gamma_n / H)\int_0^H \phi_n(z) dz$ and plotted in Figure 6a. With a fixed base condition, the first mode contributes more than 60% of the total effective mass for the flexural beam, and more than 80% for the shear beam. The second mode contributes almost 20% for the flexural beam and almost 10% for the shear beam, and the higher modes contribute the remainder. As the base fixity is released, the contribution of the first mode to the total mass increases slightly for the flexural beam and decreases slightly for the shear beam. For both beams, the first mode of the pinned-base beam contributes about 75% of the total mass and the second

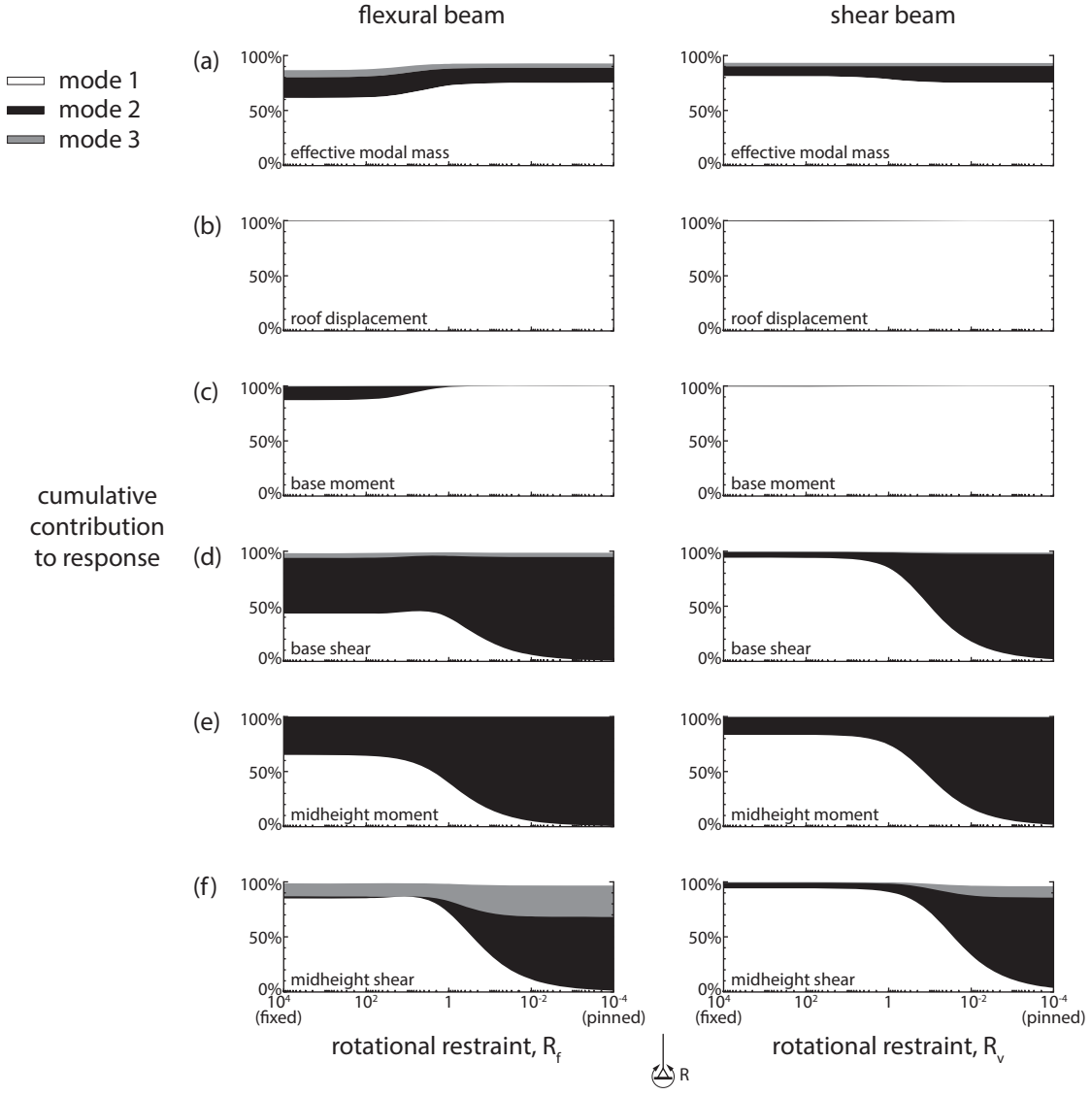

Figure 6 Cumulative modal contributions to (a) effective modal mass; (b) roof displacement; (c) base moment; (d) base shear; (e) midheight moment; (f) midheight shear. All parts except (a) assume the relative spectral shape of Figure 7.

mode contributes about 15%.

For the other response parameters that are considered in Figure 6, the relative contribution of each mode depends on the relative values of the response spectrum at each modal period. This effect is approximated within a nondimensional framework by considering a typical acceleration design spectrum based on ASCE 7-10 [2], where the relative spectral accelerations, $\overline{S}_a$, are:

$$\overline{S}_a = \begin{cases} \overline{S}_{D1}/\overline{T}_n & n \le 2 \\ \overline{S}_{D1}/\overline{T}_2 & n > 2 \end{cases} \tag{26}$$

where $\overline{S}_{D1}$ is a nondimensional spectral acceleration parameter and $\overline{T}_n$ is given in Eqs. (23)-(24). As shown in Figure 7, Eq. (26) assumes that the first mode is in the constant velocity region of the design spectrum, the second mode is at the corner of the constant velocity and constant acceleration regions, and the third and higher modes are in the constant acceleration region. If the second-mode period is in the constant acceleration region (i.e. $T_2 < T_S$, where T_S is the corner period shown in Figure 7), this assumption overestimates the influence of all higher modes. If the second-mode period is in the constant velocity region (i.e. $T_2 > T_S$), this assumption underestimates the influence of some higher modes, although it may still overestimate the influence of those modes that fall on the initial ascending branch of the design spectrum. If the first-mode period is in the constant displacement region (not shown in Figure 7), the higher modes will contribute relatively more to the overall demand, as has also been noted by Sullivan [30].

The contribution of each mode to displacements is calculated as $\Gamma_n \phi_n \overline{S}_a / \omega_n^2$, the contribution to shear forces is calculated as $\Gamma_n \overline{V}_n \overline{S}_a / \omega_n^2$, and the contribution to bending moments is calculated as $\Gamma_n \overline{M}_n \overline{S}_a / \omega_n^2$. The total contribution of the first N modes is calculated as the square root of the sum of the squares of the contributions from those modes. For each response quantity in Figure 6, the cumulative contribution of the first N modes is shown, rather than the contribution of any individual mode. All results are normalised by the total contribution from the first ten modes, and all results assume that Eq. (26) describes the relative spectral ordinates of all modes.

Figure 6b examines the contribution of each mode to the roof displacement. The first mode contributes more than 99% of the total roof displacement for both the flexural beam and the shear beam, regardless of the amount of rotational restraint at the base.

Figure 6c shows the relative importance of each mode to the base moment. For the flexural beam

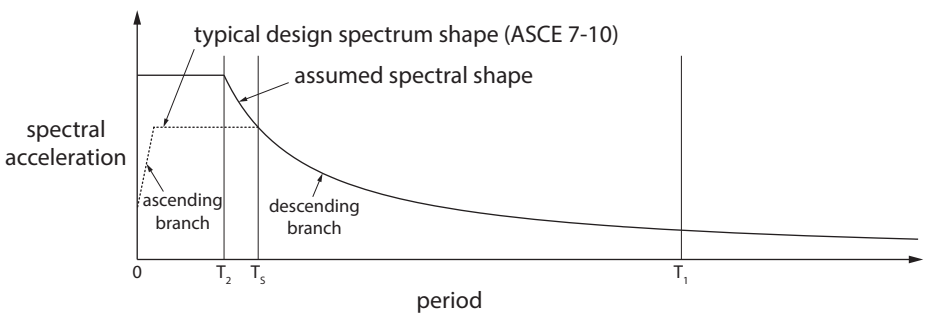

Figure 7 Assumed shape of acceleration spectrum

with a fixed base, the first mode contributes 87% of the total base moment, with almost all of the remainder coming from the second mode. As the base restraint is released, the moment contributed by all modes approaches zero, but the first mode contributes relatively more to the total. The base moment of the shear beam is almost entirely due to the first mode for any base restraint condition.

Figure 6d shows that the higher modes are relatively more significant for the base shear. The second mode contributes more than the first mode to the base shear of the flexural beam with a fixed base, and as the rotational restraint is released, the second mode dominates the response even more. For the shear beam, although the first mode contributes 94% of the base shear when the base is fixed, the second mode dominates the response as the rotational restraint at the base is released.

Considering the moment at mid-height (Figure 6e), the first mode contributes only 65% of the total when the base of the flexural beam is fixed, and as the system approaches the pinned base condition, the total mid-height moment is generated almost entirely in the second mode. For the shear beam, the first mode contributes more of the total if the base is fixed, but the second mode comes to dominate the response as the base fixity is released.

The shear at mid-height is an example of a case where the third mode contributes significantly to the response, as shown in Figure 6f. In the fixed condition for the flexural beam, the third mode adds 12% to the shear computed from the first two modes only. As the base restraint is released, the second and third modes increase in relative contribution, while the contribution from the first mode approaches zero. The third mode is less significant for the response of the shear beam.

For all of these parameters, the modal mass does not give a good indication of the relative importance of the modes: compared to what would be expected based on the relative modal masses, the higher modes contribute much less to the roof displacement and the base overturning moment, but they contribute much more to the base shear and the moments above the base. The higher modes would be even more significant if the second mode were in the constant velocity region of the assumed spectrum (Figure 7), or if the first mode were in the constant displacement region.

ACCOUNTING FOR HIGHER MODE EFFECTS IN DESIGN

The equations that were derived above can be adapted into a theory-based capacity design method for structures where the ductile mechanism is a base rotational hinge. A lateral force distribution that is consistent with the deformation profile of the system in the nonlinear range is assumed to be limited by the rotational hinge, while additional contributions are assumed based on the pinned-base higher modes that were discussed above. This approach is conceptually equivalent to the Transitory Inelastic Modes approach of Sullivan et al. [19], but unlike that study, the following section considers a simple idealized system for which closed-form equations can be derived. By using the modal properties of the idealized system, the proposed method removes the need for the designer to conduct a modal analysis of a structural model, and therefore the method is likely to be most useful for preliminary design. The following derivations are based on the assumptions that the structure behaves like a uniform shear beam above the base and that the peak response in the higher modes occurs when the base has a low rotational stiffness. Systems that cannot be characterised in this way would require approximate numerical methods or alternative mathematical derivations, such as for a flexural beam or a combined shear-flexural deformation mode.

Included modes and modal periods

Based on Figure 6, the first two lateral modes are likely to govern most response quantities of interest, but the third mode may also be significant at locations where the contribution from the second mode is small. Therefore, using the ratio of modal periods of a shear beam from Table 2, the response of a structure that behaves like a shear beam (typical low- to mid-rise buildings) may be computed using only the first three lateral modes if:

$$T_1 \leq 3T_S \tag{27}$$

where T_1 is the period of the first mode and T_S is the corner period of the acceleration spectrum, calculated according to ASCE 7-10 [2]. This assumes the spectral shape of Figure 7, which is not conservative for high-rise structures where the second-mode period is on the descending branch of the design spectrum or the first-mode period is in the constant displacement region. The requirement of Eq. (27) would be relaxed for a flexural beam, since the modes are spaced further apart (Table 2). If Eq. (27) is not satisfied, the following derivation should be extended to include additional modes. For the first design iteration, T_1 is typically estimated using an empirical equation from the building code. The higher-mode periods are not known until a design has been developed, but these periods can be estimated for any structure that is characterised by a shear beam with uniform mass and elasticity as $T_2 = T_1/3$ and $T_3 = T_1/5$. These expressions give results that are generally less conservative than using the higher-mode periods from a modal analysis with fixed base conditions, since the second- and third-mode periods are expected to be less than $T_1/3$ and $T_1/5$, respectively, if the structure behaves like a flexural beam rather than a shear beam (see Table 2). The fixed-base periods are used even in the nonlinear range because the higher-mode periods of a shear beam do not vary appreciably with the base rotational restraint (see Figure 5). The validation presented later suggests that reasonable design envelopes are obtained using these simplified period estimates, rather than the periods from modal analysis, likely because the higher-mode periods are in the constant acceleration region of the spectrum.

First-mode envelopes

The nonlinear mechanism considered in this paper is associated with a maximum expected base overturning moment, $M_{b,\max}$. This moment is greater than the rocking moment of controlled rocking systems because it includes the effects of post-tensioning elongation and strain hardening of any yielding devices that cross the base rocking joint, and it is also greater than the yield moment of reinforced concrete walls because of strain hardening of reinforcing steel. The plastic mechanism is assumed to develop due to the first-mode actions alone, as other researchers have also assumed [e.g. 19]. In this study, the deformed shape of the first mode is taken from the pinned-base structure, for which all significant first-mode deformation is due to the base rotation, resulting in an inverted triangular lateral force distribution. Alternative force distributions were also considered but found to be more complicated mathematically without a significant improvement in accuracy. If the total tributary mass of W_{trib}/g is distributed uniformly over the height H, then the total accelerations in the first mode that are associated with $M_{b,\max}$ are:

$$a_{1,\max}(z) = 3\left(\frac{M_{b,\max}/H}{W_{trib}/g}\right)\left(\frac{z}{H}\right) \tag{28}$$

where z is the height above the base. The associated shear force envelope is given by:

$$V_{1,\max}(z) = \frac{3}{2}\left(\frac{M_{b,\max}}{H}\right)\left[1-\left(\frac{z}{H}\right)^2\right] \tag{29}$$

Similarly, the first-mode overturning moment envelope is:

$$M_{1,\max}(z) = M_{b,\max}\left[1-\frac{3}{2}\left(\frac{z}{H}\right)+\frac{1}{2}\left(\frac{z}{H}\right)^2\right] \tag{30}$$

These envelopes are plotted in Figure 8.

Higher-mode envelopes

For each of the higher modes, the following derivation uses the five-percent-damped acceleration spectrum. Further study may refine this assumed damping value or show that systems with energy dissipation distributed over the height can benefit from increased damping in the higher modes.

Using Eq. (4), the total acceleration in mode n is:

$$a_n(z,t) = \phi_n(z)\Gamma_n A_n(t) \tag{31}$$

where $A_n(t)$ is the total acceleration of the SDOF system with the properties of mode n. The spectral displacement at a period of T_n and with the damping of mode n, $S_d(T_n)$, is related to the pseudo-spectral acceleration, $S_a(T_n)$, by:

$$S_a(T_n) = \omega_n^2 S_d(T_n) \tag{32}$$

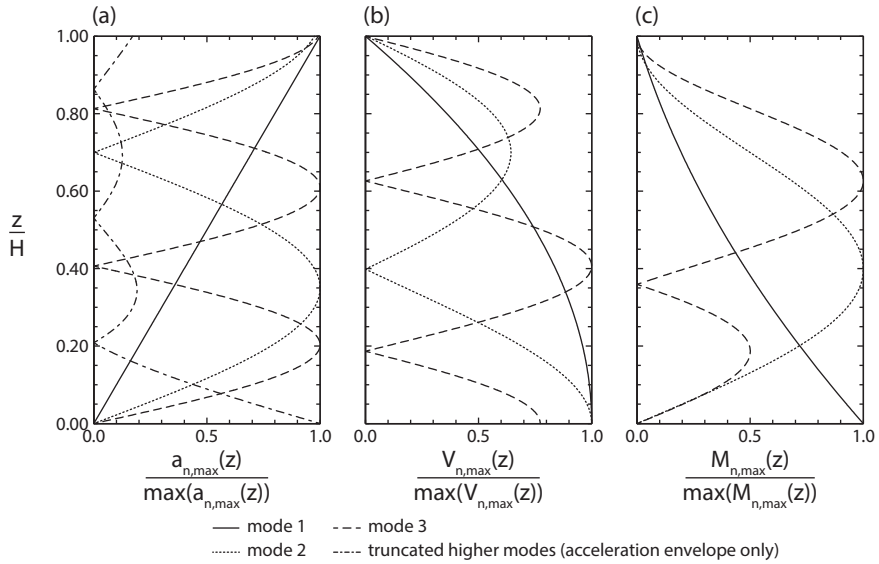

Figure 8 Shapes of modal contributions: (a) acceleration; (b) storey shear; (c) overturning moment

This is approximately equal to the maximum absolute value of $A_n(t)$, except for long periods or large damping [27].

Evaluating Eq. (18) for the mode shape $\phi_n(z)$ of a shear beam that is given in Eq. (16):

$$\Gamma_n = \frac{4(1-\cos\beta_n H)}{C_n(2\beta_n H - \sin 2\beta_n H)} \tag{33}$$

where $\beta_n H$ is given for pinned-base and fixed-base shear beams in Table 1, and where C_n is an arbitrary constant that also appears in the numerator of $\phi_n(z)$.

Using the mode shape from Eq. (16) together with Eq. (33), the maximum acceleration profile along the height of the structure in mode n can be found from Eq. (31) as:

$$a_{n,\max}(z) = \left|\sin\beta_n z\left[\frac{4(1-\cos\beta_n H)}{2\beta_n H - \sin 2\beta_n H}\right]\right| S_a(T_n) \tag{34}$$

Table 3 simplifies Eq. (34) using $\beta_n H$ for the second and third pinned-base shear beam modes from Table 1. Eq. (34) is plotted in Figure 8a for the second and third modes. For each mode n, the plot is normalised by the maximum value of $a_{n,\max}(z)$ over all values of z. The equations in Table 3 and the shapes in Figure 8a assume a shear beam with uniform mass and stiffness, but no assumptions regarding the spectral shape or modal periods are necessary.

In a similar manner, using Eqs. (12), (14), (16), and (21), and replacing ρAH with W_{trib}/g, the contribution of each higher mode to the shear force envelope can be shown to be:

$$V_{n,\max}(z) = \left(\frac{W_{trib}}{g}\right) S_a(T_n)\left|\left[\frac{4(1-\cos\beta_n H)}{2\beta_n H - \sin 2\beta_n H}\right]\left(\frac{\cos\beta_n z - \cos\beta_n H}{\beta_n H}\right)\right| \tag{35}$$

Table 3 simplifies Eq. (35) using $\beta_n H$ for the second and third pinned-base shear beam modes from Table 1, and these equations are plotted in Figure 8b. For each mode n, the plot is normalised by the maximum value of $V_{n,\max}(z)$.

Similarly, it can be shown that the maximum overturning moment in mode n is:

$$M_{n,\max}(z) = \frac{(W_{trib}/g)S_a(T_n)}{(\beta_n H)^2}\left|\left[\frac{4(1-\cos\beta_n H)}{2\beta_n H - \sin 2\beta_n H}\right](\beta_n z\cos\beta_n H - \sin\beta_n z)\right| \tag{36}$$

Table 3 simplifies Eq. (36) by using $\beta_n H$ for the second and third modes from Table 1, and these equations are plotted in Figure 8c. For each mode n, the plot is normalised by the maximum value of $M_{n,\max}(z)$.

Because each modal contribution in Figure 8 is normalised by the maximum value in that mode, Figure 8 does not represent the relative contributions of the different modes.

Table 3 Summary of modal contributions to design envelopes

description	equation
storey shear	
first mode	$V_{1,\max}(z) = \frac{3}{2}\left(\frac{M_{b,\max}}{H}\right)\left[1-\left(\frac{z}{H}\right)^2\right]$
second mode	$V_{2,\max}(z) = 0.1265\left[S_a(T_1/3)\right]\left(\frac{W_{trib}}{g}\right)\left\lvert\cos 4.49\left(\frac{z}{H}\right)+0.217\right\rvert$
third mode	$V_{3,\max}(z) = 0.0297\left[S_a(T_1/5)\right]\left(\frac{W_{trib}}{g}\right)\left\lvert\cos 7.73\left(\frac{z}{H}\right)-0.1283\right\rvert$
overturning moment	
first mode	$M_{1,\max}(z) = M_{b,\max}\left[1-\frac{3}{2}\left(\frac{z}{H}\right)+\frac{1}{2}\left(\frac{z}{H}\right)^2\right]$
second mode	$M_{2,\max}(z) = 0.0282\left[S_a(T_1/3)\right]\left(\frac{W_{trib}}{g}\right)H\left\lvert\sin 4.49\left(\frac{z}{H}\right)+0.976\left(\frac{z}{H}\right)\right\rvert$
third mode	$M_{3,\max}(z) = 0.00384\left[S_a(T_1/5)\right]\left(\frac{W_{trib}}{g}\right)H\left\lvert\sin 7.73\left(\frac{z}{H}\right)-0.991\left(\frac{z}{H}\right)\right\rvert$
floor acceleration	
first mode	$a_{1,\max}(z) = 3\left(\frac{M_{b,\max}/H}{W_{trib}/g}\right)\left(\frac{z}{H}\right)$
second mode	$a_{2,\max}(z) = 0.569S_a(T_1/3)\left\lvert\sin 4.49\left(\frac{z}{H}\right)\right\rvert$
third mode	$a_{3,\max}(z) = 0.229S_a(T_1/5)\left\lvert\sin 7.73\left(\frac{z}{H}\right)\right\rvert$
residual	$a_{r,\max}(z) = \left\lvert 1-\frac{3}{2}\left(\frac{z}{H}\right)-0.569\sin 4.49\left(\frac{z}{H}\right)-0.229\sin 7.73\left(\frac{z}{H}\right)\right\rvert PGA$

Notation: $M_{b,\max}$ = overstrength base overturning moment, z = height above base, H = total height, W_{trib}/g = total tributary mass, PGA = peak ground acceleration, $S_a(T)$ = spectral acceleration at period T, where the elastic first-mode period is T_1 and the second- and third-mode periods for the pinned-base beam are assumed to be $T_1/3$ and $T_1/5$, respectively.

Combination of modal envelopes

To combine the modal contributions from Table 3, the peak forces are assumed to develop in the first mode and to remain nearly constant while the higher modes oscillate. Based on this assumption, the design storey shears and overturning moments are taken as the sum of the respective absolute values from the first mode with the square root of the sum of the squares (SRSS) from the higher modes. The SRSS method is used for its simplicity and because the modal periods of a cantilever beam are well separated. Including the first-mode effects under the square root was

found to be unconservative for the controlled rocking steel braced frames that were considered. When three modes are used, these combinations are written as:

$$V_{\max}(z) = V_{1,\max}(z) + \sqrt{(V_{2,\max}(z))^2 + (V_{3,\max}(z))^2} \tag{37}$$

$$M_{\max}(z) = M_{1,\max}(z) + \sqrt{(M_{2,\max}(z))^2 + (M_{3,\max}(z))^2} \tag{38}$$

To calculate the design peak floor accelerations, a combination similar to Eqs. (37)-(38) gives an acceleration of zero at the base, where the peak acceleration must equal the peak ground acceleration. Pozzi and Der Kiureghian [31] have explained this by showing that the peak accelerations near the base are dominated by the rigid response of the structure, which is not captured when only the first few modes are used. To correct for the error associated with truncating the higher modes, they proposed a modification of the complete quadratic combination (CQC) method. Their proposal is simplified for this capacity design method, so as to combine the modal contributions in a way that is consistent with what was suggested for the shear force and overturning moment envelopes. Thus, the peak floor acceleration at each level is estimated as:

$$a_{\max}(z) = a_{1,\max}(z) + \sqrt{(a_{2,\max}(z))^2 + (a_{3,\max}(z))^2} + a_{r,\max}(z) \tag{39}$$

The residual acceleration envelope associated with the truncated higher modes, $a_{r,\max}(z)$, is calculated using the following equation, which is derived by Pozzi and Der Kiureghian [31]:

$$a_r(z) = \left[1 - \sum_{n=1}^{N} \Gamma_n \phi_n(z)\right] a_g(t) \tag{40}$$

where $a_g(t)$ is the horizontal ground acceleration and N is the number of modes that are considered directly when computing the acceleration envelope (e.g. three in Eq. (39)). Based on the assumed properties for the first three modes that were described above, the terms in Eq. (40) are found from the acceleration profiles in Table 3. Taking the maximum absolute value of Eq. (40) gives the maximum residual acceleration envelope associated with the truncated higher modes:

$$a_{r,\max}(z) = \left|1 - 1.5\left(\frac{z}{H}\right) - 0.569\sin 4.49\left(\frac{z}{H}\right) - 0.229\sin 7.73\left(\frac{z}{H}\right)\right| \times PGA \tag{41}$$

where PGA is the peak horizontal ground acceleration. Eq. (41) is plotted in Figure 8a, normalised by the maximum value of $a_{r,\max}(z)$. As noted earlier, Figure 8a does not represent the relative contributions of the different modes. Because Eq. (41) was developed by assuming that the first three modes are included in Eq. (39), it must be modified if a different number of modes is used.

VALIDATION OF PROPOSED DESIGN EQUATIONS FOR CONTROLLED ROCKING STEEL BRACED FRAMES

Comparison with shake table testing

Figure 9a shows a schematic of a 30% scale model of an eight-storey controlled rocking steel braced frame that was tested on a shake table [24-25]. The frame was scaled from a design for an

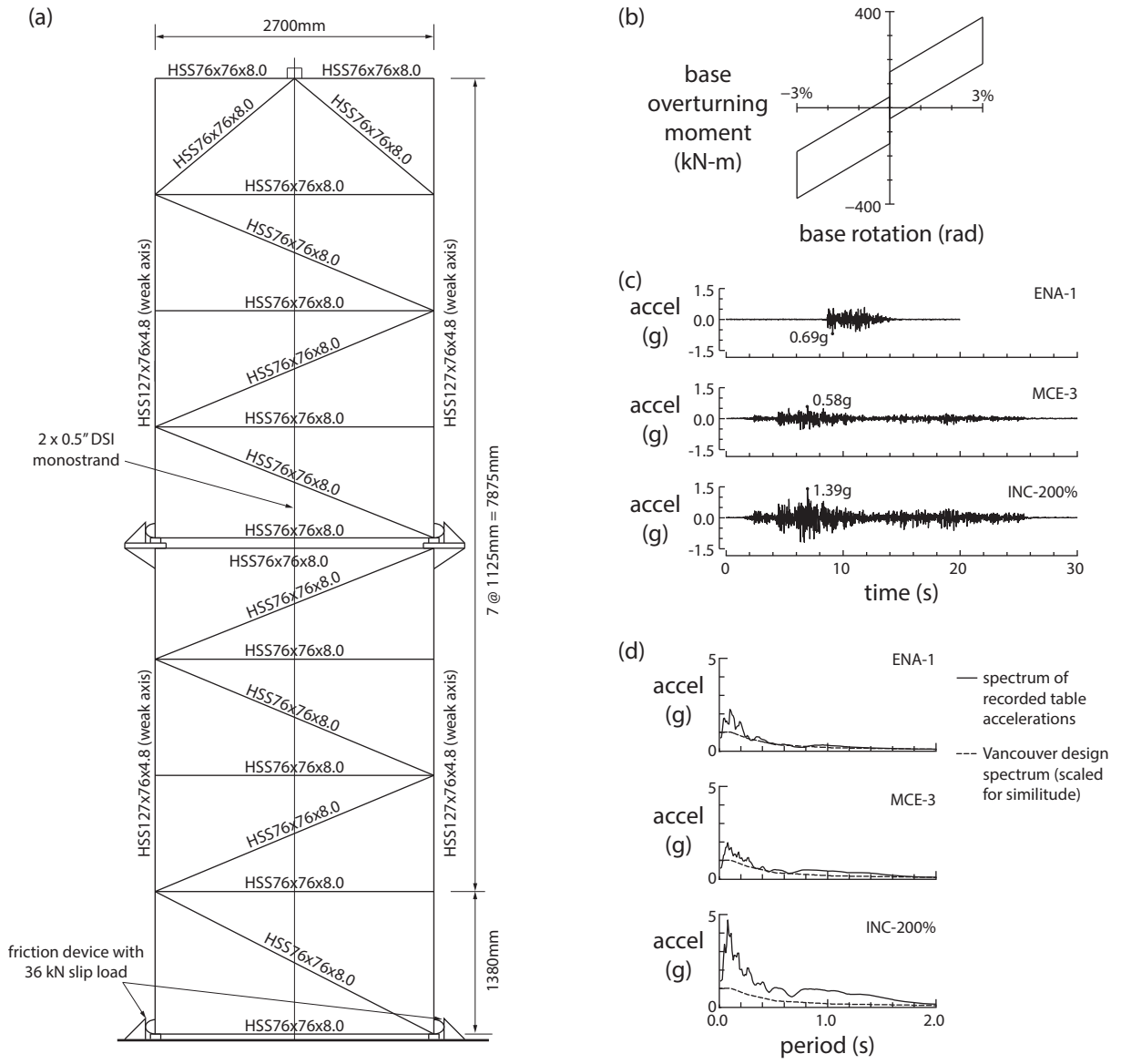

Figure 9 Shake table test structure: (a) schematic; (b) theoretical base moment-rotation response; (c) recorded table accelerations; (d) 5%-damped acceleration spectra of recorded table accelerations

eight-storey building in Vancouver. Post-tensioning and friction energy dissipation were provided, resulting in the theoretical base moment-rotation response that is shown in Figure 9b. The first-mode period of the structure was measured as 0.49 s using low-amplitude testing that did not cause base uplift. Figure 9c shows the recorded table accelerations for three records where the higher modes had a relatively significant influence on the response, and Figure 9d shows the associated response spectra. The design spectrum for the Vancouver site is shown for reference. Both the design spectrum and the ground motions were scaled to satisfy similitude requirements. The 19 ground motions that were used for testing are described by Wiebe et al. [24-25].

For the three ground motions that are shown in Figure 9c, Figure 10 compares the measured peak overturning moments, storey shears, and floor accelerations to the values calculated using the

proposed method. These calculations use the response spectra of the recorded ground motions with 5% damping because this was consistent with the measured response [32]. The maximum base moment is taken as the value that was measured during each test, whereas for capacity design purposes, it would be taken as the maximum expected overstrength base moment. The initial period was taken from the experimental results, but no modal analysis was required for the proposed

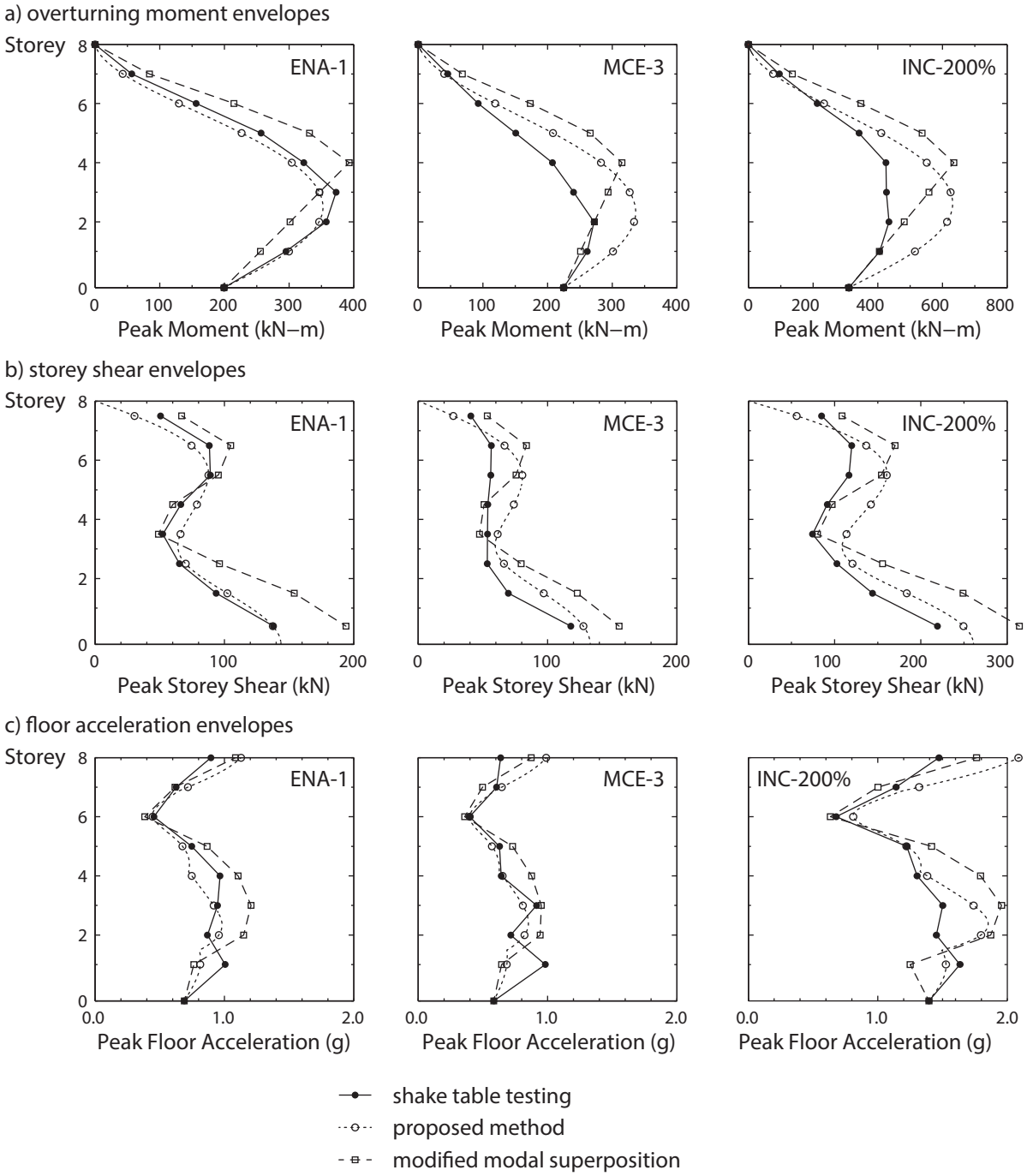

Figure 10 Envelopes for records ENA-1, MCE-3, and INC-200%: (a) overturning moment; (b) storey shear; (c) floor acceleration

method. For comparison, a modified modal superposition (MMS) approach based on the recommendations of Priestley and Amaris [8] is also shown. In this method, the first-mode demands are calculated in the same way as above, assuming an inverted triangular distribution of forces to reach the maximum measured base overturning moment, but the higher-mode contributions are calculated from an elastic modal analysis of a simple model that was made in SAP2000 [33] and used for design [32]. The first-mode period of this model was 0.44 s, compared to a measured period of 0.49 s. The first three modes are used, accounting for 98% of the mass participation, together with the 5% damped spectra of the measured ground motions. As recommended by Priestley and Amaris [8], the modal contributions to overturning moment in the top half of the structure are combined using the SRSS and multiplied by 1.1, while the moment envelope in the bottom half is taken as linear from the estimate at the fourth storey to the known maximum base overturning moment. The modal contributions to storey shears are combined using the SRSS, and the same assumption is also used to calculate an acceleration envelope.

Figure 10a shows that the proposed method captures the shape of the overturning moment envelope reasonably well. Although this method calculates the peak overturning moment over the height to within 5% for record ENA-1, which had particularly strong higher mode effects because of its high-frequency content, the method is conservative by more than 20% for the other two records that are shown. The MMS method is more conservative and less accurate than the proposed method in the upper half of the frame for each of the three tests that are shown, but the MMS method is less conservative than the proposed method in the lower half of the frame, making it less accurate for record ENA-1 but more accurate for the other two records. Table 4 gives the ratio of the maximum calculated overturning moment over the height to the maximum measured moment

Table 4 Ratios of estimated to measured response parameters

	Maximum Overturning Moment over Height		**First-Storey Shear**		**Peak Floor Acceleration**	
ground motion	**proposed method**	**modified modal superposition**	**proposed method**	**modified modal superposition**	**proposed method**	**modified modal superposition**
SLE-1	1.00	1.00	1.32	1.21	0.93	0.72
SLE-2	1.00	1.00	1.28	0.88	1.07	0.57
DBE-1	1.00	1.00	1.18	1.62	0.73	0.91
DBE-2	1.00	1.00	1.31	1.45	0.98	0.93
DBE-3	1.00	1.00	1.15	1.07	0.92	0.77
CAS-1	1.11	1.00	1.20	0.99	0.99	0.71
CAS-2	1.09	1.26	1.05	1.67	0.81	1.10
ENA-1	0.95	1.05	1.03	1.41	1.12	1.20
ENA-2	1.42	1.69	1.06	1.55	1.01	1.19
MCE-1	1.00	0.95	1.31	1.69	0.81	0.86
MCE-2	1.36	1.10	1.22	1.24	1.02	0.87
INC-25%	1.00	1.00	1.22	1.14	1.06	0.83
INC-50%	1.10	1.00	1.01	0.99	0.78	0.66
INC-75%	1.17	0.95	1.13	1.17	0.90	0.78
INC-100% (= MCE-3)	1.24	1.16	1.11	1.32	1.01	0.97
INC-125%	1.33	1.25	1.31	1.53	1.11	1.05
INC-150%	1.22	1.37	1.18	1.65	1.15	1.25
INC-175%	1.38	1.43	1.24	1.56	1.08	1.07
INC-200%	1.45	1.46	1.17	1.43	1.28	1.20
mean	**1.14**	**1.13**	**1.18**	**1.34**	**0.97**	**0.92**
st. dev.	**0.15**	**0.20**	**0.10**	**0.26**	**0.12**	**0.19**

for all 19 ground motions that were tested. The proposed method, which does not require a modal analysis, is only slightly more conservative than the modified modal superposition (average of 1.14 compared to 1.13), with a slightly smaller sample standard deviation (0.15 compared to 0.20).

For the three records that are shown in Figure 10b, the proposed method captures the shape of the experimentally measured shear force envelopes well, including the relative reduction that occurs below midheight of the frame. The peak first-storey shear is captured to within 3% for record ENA-1, and within 17% for the other two records. The MMS method also captures the reduction in shear near midheight, but the first-storey shear is overestimated by more than 32% for all three records shown because it is based on the fixed-base modes (see Figure 3 and Figure 4). Even when considering ground motions where the higher modes have relatively less effect, Table 4 shows that the proposed method captures the first-storey shear more accurately than the MMS method (average error of 18% on the conservative side, compared to 34%) and with a reduced sample standard deviation (0.10 compared to 0.26), while also avoiding the need for a modal analysis.

The estimated acceleration envelopes have a more complex shape than the other envelopes because the higher modes contribute more significantly to this parameter. For records ENA-1 and MCE-3, the acceleration envelopes computed using the proposed method are accurate to within 30% at all levels, while those calculated using the MMS method are within 37% at all levels, with both methods overestimating the accelerations at some levels and underestimating them at others. The error is similar for record INC-200% at all levels except the top, where both methods overestimate the peak acceleration. Even though the peak floor accelerations are not computed very accurately at individual levels, Table 4 shows that both methods capture the peak floor acceleration at all levels to within 8% accuracy on average.

Comparison with nonlinear time history analyses

Additional validation has been completed using nonlinear time history analyses of controlled rocking steel braced frames with two, six, and 12 storeys [34]. The frames were designed using a performance-based approach and were subjected to a suite of 44 records at the Maximum Considered Earthquake (MCE) level. The acceleration, shear force, and overturning moment envelopes were estimated using the method proposed here. To conservatively estimate the influence of the higher modes, the acceleration spectrum in Table 3 was taken as one standard deviation above the median of the ground motion suite. For the six- and 12-storey frames, the estimates of all three response quantities were generally one standard deviation above the median response, to within about 10%. However, the equations presented here overestimated the peak shears and overturning moments for the two-storey frame during all 44 ground motions. This unnecessary conservatism is because the mass is not uniformly distributed over the height for such a low-rise structure. Similar accuracy was found when considering the peak floor accelerations [32].

CONCLUSION

Higher mode effects work against the goal of capacity-based seismic design by allowing peak seismic forces to increase even after a nonlinear mechanism has formed. To study the response of the structures that are most influenced by higher mode effects, an analogy was made to a cantilever shear or flexural beam with a variable amount of base rotational restraint. Solving for the modal properties of these beams showed that the first mode changes significantly as the base condition

changes from fixed to pinned, but the higher modes are less affected: the periods of the higher modes elongate, but this elongation is bounded, is small for the shear beam, and decreases with increasing mode number for the flexural beam. The modal shear force and overturning moment diagrams change with the amount of base fixity, so the fixed-base modes may not capture the real higher-mode response. Assuming that the first mode is in the constant velocity region of a typical design spectrum while the higher modes are in the constant acceleration region, most response quantities of interest are controlled by the first two lateral modes only, regardless of the base fixity, except at locations along the height where the second mode contributes little.

Using the analogy of a uniform cantilever shear beam, closed-form expressions were developed to estimate the modal overturning moment, storey shear, and floor acceleration envelopes, using only the tributary weight, structural height, acceleration spectrum, and an estimate of the first-mode period. These expressions can easily be implemented in a spreadsheet, allowing a designer to estimate the system forces for preliminary design without conducting any modal analysis. Relative to the envelopes that were measured during large-scale shake table testing of a controlled rocking steel braced frame, the proposed method was of similar or better accuracy to a modal superposition approach, but it avoided the need for modal analysis of a structural model. Nonlinear time history analyses of other designs have further confirmed the validity of the proposed approach [34]. Although the analogy in this paper to a beam with uniformly distributed mass is not appropriate for low-rise buildings, higher mode effects are not generally significant for these structures.

This paper was developed as part of a study of controlled rocking steel braced frames. Although it is expected to apply to other systems that rely on a nonlinear moment-rotation response at the base to limit the peak forces, further analysis is required to verify this. Future work will also extend the expressions that have been developed based on the properties of cantilevered shear beams to encompass the spectrum between shear and flexural beams.

ACKNOWLEDGEMENTS

This project was funded by the Natural Sciences and Engineering Research Council of Canada, the Canadian Seismic Research Network, and the Ontario Ministry of Research and Innovation.

REFERENCES

1. Park R, Paulay T. 1975. *Reinforced concrete structures*. New York, NY: John Wiley & Sons, Inc.
2. ASCE (American Society of Civil Engineers). 2010. *Minimum design loads for buildings and other structures*. ASCE Standard ASCE/SEI 7-10. Reston, VA: American Society of Civil Engineers.
3. Priestley MJN, Calvi GM, Kowalsky MJ. 2007. *Displacement-based seismic design of structures*. Pavia, Italy: IUSS Press.
4. Blakeley RWG, Cooney RC, Meggett LM. 1975. Seismic shear loading at flexural capacity in cantilever wall structures. *Bulletin of the New Zealand Society for Earthquake Engineering*, 8(4): 278-290.
5. Filiatrault A, D'Aronco D, Tinawi R. 1994. Seismic shear demand of ductile cantilever walls: a Canadian code perspective. *Canadian Journal of Civil Engineering*, 21(3): 363-376.
6. Seneviratna GDPK, Krawinkler H. 1994. Strength and displacement demands for seismic design of structural walls. *Proceedings of the 5th US National Conference on Earthquake Engineering*, Chicago, IL.
7. Tremblay R, Léger P, Tu J. 2001. Inelastic seismic response of concrete shear walls considering P-delta effects. *Canadian Journal of Civil Engineering*, 28(4): 640-655.
8. Priestley MJN, Amaris AD. 2002. Dynamic amplification of seismic moments and shear forces in cantilever walls. *ROSE Report 2002/01*. Pavia, Italy: IUSS Press.
9. Rad BR, Adebar P. 2008. Dynamic shear amplification in high-rise concrete walls: effect of multiple flexural

hinges and shear cracking. *14th World Conference on Earthquake Engineering*, Beijing, China.
10. Panneton M, Léger P, Tremblay R. 2006. Inelastic analysis of a reinforced concrete shear wall building according to the National Building Code of Canada. *Canadian Journal of Civil Engineering*, 33(7): 854-871.
11. Boivin Y, Paultre P. 2012. Seismic force demand on ductile reinforced concrete shear walls subjected to western North American ground motions: Part 1 - parametric study. *Canadian Journal of Civil Engineering*, 39(7): 723-737.
12. Eberhard MO, Sozen MA. 1993. Behavior-based method to determine design shear in earthquake-resistant walls. *Journal of Structural Engineering*, 119(2): 619-640.
13. Panagiotou M, Restrepo JI. 2011. Displacement-based method of analysis for regular reinforced-concrete wall buildings: application to a full-scale 7-story building slice tested at UC-San Diego. *Journal of Structural Engineering*, 137(6): 677-690.
14. Ghorbanirenani I, Tremblay R, Léger P, Leclerc M. 2012. Shake table testing of slender RC shear walls subjected to eastern North America seismic ground motions. *Journal of Structural Engineering*, 138(12): 1515-1529.
15. Rutenberg A. 2013. Seismic shear forces on RC walls: review and bibliography. *Bulletin of Earthquake Engineering*, 11(5): 1726-1751.
16. Eibl J, Keintzel E. 1988. Seismic shear forces in RC cantilever shear walls. *9th World Conference on Earthquake Engineering*, Tokyo and Kyoto, Japan.
17. Keintzel E. 1992. Advances in the design for shear of RC structural walls under seismic loading. *Nonlinear Seismic Analysis and Design of Reinforced Concrete Buildings*, ed. P. Fajfar and H. Krawinkler, New York, NY: Elsevier Science Publishers Ltd.
18. Kowalsky MJ. 2002. A displacement-based approach for the seismic design of continuous concrete bridges. *Earthquake Engineering and Structural Dynamics*, 31(3): 719-747.
19. Sullivan TJ, Priestley MJN, Calvi GM. 2008. Estimating the higher-mode response of ductile structures. *Journal of Earthquake Engineering*, 12(3): 456-472.
20. Pennucci D, Sullivan TJ, Calvi GM. 2014. Inelastic higher-mode response in reinforced concrete wall structures. *Earthquake Spectra*, in press, DOI 0.1193/051213EQS123M.
21. Roke D, Sause R, Ricles JM, Gonner N. 2009. Damage-free seismic-resistant self-centering steel concentrically braced frames. *6th International Conference on Behaviour of Steel Structures in Seismic Areas (STESSA 2009)*, Philadelphia, PA.
22. Eatherton M, Hajjar J. 2010. Large-scale cyclic and hybrid simulation testing and development of a controlled-rocking steel building system with replaceable fuses. *NSEL Report NSEL-025*. Urbana, IL: Department of Civil and Environmental Engineering, University of Illinois at Urbana-Champaign.
23. Ma X. 2010. Seismic design and behavior of self-centering braced frame with controlled rocking and energy-dissipating fuses. *PhD Dissertation*. Stanford, CA: Stanford University.
24. Wiebe L, Christopoulos C, Tremblay R, Leclerc M. 2013. Mechanisms to limit higher mode effects in a controlled rocking steel frame. 1: Concept, modelling, and low-amplitude shake table testing. *Earthquake Engineering and Structural Dynamics*, 42(7): 1053-1068.
25. Wiebe L, Christopoulos C, Tremblay R, Leclerc M. 2013. Mechanisms to limit higher mode effects in a controlled rocking steel frame. 2: Large-amplitude shake table testing. *Earthquake Engineering and Structural Dynamics*, 42(7): 1069-1086.
26. Timoshenko SP. 1921. On the correction for shear of the differential equation for transverse vibrations of prismatic bars. *Philosophical Magazine*, Series 6, 41(245): 744-746.
27. Chopra AK. 2012. *Dynamics of structures: theory and applications to earthquake engineering. 4th ed*. Upper Saddle River, NJ: Prentice Hall.
28. Miranda E. 1999. Approximate seismic lateral deformation demands in multistory buildings. *Journal of Structural Engineering*, 125(4): 417-425.
29. Young D, Felgar RP. 1949. Tables of Characteristic Functions Representing Normal Modes of Vibration of a Beam. Publication 4913, Austin, TX: University of Texas.
30. Sullivan TJ. 2010. Capacity design considerations for RC frame-wall structures. *Earthquakes and Structures*, 1(4): 391-410.
31. Pozzi M, Der Kiureghian A. 2012. Response spectrum analysis for floor acceleration. *15th World Conference on Earthquake Engineering*, Lisbon, Portugal.
32. Wiebe L. 2013. Design of controlled rocking steel frames to limit higher mode effects. *PhD Thesis*. Toronto, ON: University of Toronto, ON.
33. Computers and Structures, Inc. 2009. SAP2000 Advanced 14.0.0: Structural analysis program. Berkeley, CA: Computers and Structures, Inc.
34. Wiebe L, Christopoulos C. Under review. Performance-based design of controlled rocking steel braced frames. 2: Design of capacity-protected elements. Revision submitted to *Journal of Structural Engineering* in June 2014.